Behavioral/Cognitive

Contingent Amygdala Inputs Trigger Heterosynaptic LTP at Hippocampus-To-Accumbens Synapses

Jun Yu,[1] Susan R. Sesack,[1,2] Yanhua Huang,[1] Oliver M. Schlüter,[1] Anthony A. Grace,[1,2,3] and Yan Dong[1,2]
[1]Department of Neuroscience, University of Pittsburgh, Pittsburgh, Pennsylvania 15260, [2]Department of Psychiatry, University of Pittsburgh School of Medicine, Pittsburgh, Pennsylvania 15260, and [3]Department of Psychology, University of Pittsburgh, Pittsburgh, Pennsylvania 15260

The nucleus accumbens shell (NAcSh) is a key brain region where environmental cues acquire incentive salience to reinforce motivated behaviors. Principal medium spiny neurons (MSNs) in the NAcSh receive extensive glutamatergic projections from limbic regions, among which, the ventral hippocampus (vH) transmits information enriched in contextual cues, and the basolateral amygdala (BLA) encodes real-time arousing states. The vH and BLA project convergently to NAcSh MSNs, both activated in a time-locked manner on a cue-conditioned motivational action. In brain slices prepared from male and female mice, we show that co-activation of the two projections induces long-term potentiation (LTP) at vH-to-NAcSh synapses without affecting BLA-to-NAcSh synapses, revealing a heterosynaptic mechanism through which BLA signals persistently increase the temporally contingent vH-to-NAcSh transmission. Furthermore, this LTP is more prominent in dopamine D1 receptor-expressing (D1) MSNs than D2 MSNs and can be prevented by inhibition of either D1 receptors or dopaminergic terminals in NAcSh. This heterosynaptic LTP may provide a dopamine-guided mechanism through which vH-encoded cue inputs that are contingent to BLA activation acquire increased circuit representation to reinforce behavior.

Key words: **amygdala; dopamine; heterosynaptic; hippocampus; LTP; nucleus accumbens**

Significance Statement

In motivated behaviors, environmental cues associated with arousing stimuli acquire increased incentive salience, processes mediated in part by the nucleus accumbens (NAc). NAc principal neurons receive glutamatergic projections from the ventral hippocampus (vH) and basolateral amygdala (BLA), which transmit information encoding contextual cues and affective states, respectively. Our results show that co-activation of the two projections induces long-term potentiation (LTP) at vH-to-NAc synapses without affecting BLA-to-NAc synapses, revealing a heterosynaptic mechanism through which BLA signals potentiate the temporally contingent vH-to-NAc transmission. Furthermore, this LTP is prevented by inhibition of either D1 receptors or dopaminergic axons. This heterosynaptic LTP may provide a dopamine-guided mechanism through which vH-encoded cue inputs that are contingent to BLA activation acquire increased circuit representation to reinforce behavior.

Introduction

In motivated behaviors, environmental cues associated with arousing stimuli acquire increased incentive salience, contributing to cue-conditioned reinforcement. Such cue-reinforced responses not only encourage animals to pursue reward and flee from danger in response to predicting signs but are also implicated in psychiatric conditions, such as cue-induced relapse in substance use disorder and posttraumatic stress disorder (Volkow et al., 2017). Glutamatergic projections from limbic and paralimbic brain regions transmit related but distinct cue and motivation information that converges onto individual principal medium spiny neurons (MSNs) in the nucleus accumbens (NAc; French and Totterdell, 2002, 2003; Xia et al., 2020). During cue-conditioned responses, these projections may interactively influence each other, with the resulting circuit plasticity critical for cue-stimulus conditioning (Sesack and Grace, 2010; Belujon and Grace, 2011; Gill and Grace, 2011). To start to understand these circuit mechanisms, the current study focused on heterosynaptic interaction between two projections to NAc MSNs, one from the ventral hippocampus (vH) and the other from the basolateral amygdala (BLA).

Both vH and BLA neurons project to the NAc and form glutamatergic synapses on the same dendrites of MSNs (French and Totterdell, 2002, 2003; Britt et al., 2012; Xia et al., 2020). In behaving animals, vH neurons are preferentially activated

Received Apr. 30, 2022; revised June 14, 2022; accepted July 7, 2022.

Author contributions: J.Y., S.R.S., Y.H., O.M.S., A.A.G., and Y.D. designed research; J.Y. performed research; J.Y. analyzed data; J.Y. wrote the first draft of the paper; J.Y., S.R.S., Y.H., O.M.S., and A.A.G. edited the paper; Y.D. wrote the paper.

This work was partially supported by National Institutes of Health Grants DA46491 (to Y.H.), DA46346 (to Y.H.), DA023206 (to Y.D.), DA040620 (to Y.D.), DA047861 (to Y.D.), DA051010 (to Y.D.), MH 57440 (to A.A.G.), and NS107604 (to O.M.S.). We thank Min Lin for excellent technical support.

The authors declare no competing financial interests.

Correspondence should be addressed to Yan Dong at yandong@pitt.edu or Jun Yu at junyu005@126.com.

https://doi.org/10.1523/JNEUROSCI.0838-22.2022

by contextual cues, particularly those associated with motivational components (Wolosin et al., 2012; Bladon et al., 2019; Trouche et al., 2019; van de Ven et al., 2020; Klee et al., 2021; Smith et al., 2022). On the other hand, BLA neurons are activated by both unconditioned and conditioned stimuli with different valences (Gore et al., 2015; Janak and Tye, 2015; Corder et al., 2019; X. Zhang et al., 2021). It has been hypothesized that a key function of the BLA is to assign an incentive value to a given conditioning cue (Weymar and Schwabe, 2016). Consistent with this view, inhibition of the BLA or BLA-to-NAc projection before cue-conditioning disrupts the acquisition of cue-conditioned responding (O'Neill et al., 2018).

Monosynaptic long-term potentiation (LTP) or long-term depression (LTD) can be induced at vH-to-NAc or BLA-to-NAc synapses when patterned stimulations are applied exclusively to the vH-to-NAc or BLA-to-NAc projection (Uno and Ozawa, 1991; Dong et al., 2007; Lee et al., 2013; Ji et al., 2015; LeGates et al., 2018; Zinsmaier et al., 2022). These monosynaptic forms of synaptic plasticity suggest that each of the vH-to-NAc and BLA-to-NAc projection possesses the capacity of independently changing its transmission efficacy during behavioral responses. During cue-conditioned motivated responding, the vH and BLA are activated simultaneously, allowing vH-to-NAc and BLA-to-NAc synapses to be activated in a largely synchronous manner (Jarzebowski et al., 2022). To explore the potential heterosynaptic interaction between these two projections in the NAc shell (NAcSh), a subregion of the NAc critically implicated in cue-stimulus association, we employed a dual-rhodopsin system to optogenetically stimulate vH and BLA projections in brain slices and recorded their respective synaptic responses in the same MSNs. A brief (eight times/2 min) co-activation of the two projections induced LTP at vH-to-NAcSh synapses without affecting BLA-to-NAcSh synapses, revealing a timing-dependent, heterosynaptic mechanism through which BLA-to-NAcSh inputs persistently increased the vH-to-NAcSh transmission. Furthermore, this LTP was more prominent in dopamine D1 receptor-expressing (D1) MSNs than D2 MSNs and was prevented by either pharmacological inhibition of D1 receptors or chemogenetic inhibition of midbrain-originated dopaminergic terminals, indicating dopamine as an essential third party for enabling this heterosynaptic LTP. This heterosynaptic LTP may provide a dopamine-determinant mechanism through which vH-encoded cue inputs that are contingent to BLA activation acquire increased circuit representation, contributing to cue-reinforced behavior.

Materials and Methods

Subjects and reagents

Both male and female C57B/6J wild-type mice (purchased from Charles River) and transgenic mice (D1-tdTomato and DAT-Cre, in house bred) were grouped and allocated for planned experiments at the age of six to eight weeks. Mice were singly housed on a regular 12/12 h light/dark cycle (light on/off at 7 A.M./7 P.M.), with food and water available *ad libitum*. After acclimation, surgery, and postsurgery recovery, mice at approximately three months old were used to prepare brain slices. The animals were used in accordance with the National Institutes of Health *Guide for Experimental Animal Use* and under protocols approved by the Institutional Animal Care and Use Committee at the University of Pittsburgh. rAAV2/hSyn-hChR2(H134R)-EYFP-WPRE-PA and rAAV8/syn-ChR-88m19-tdT (Chrimson) were purchased from the University of North Carolina Vector Core, and pAAV-hSyn-DIO-hM4D(GI)-mCherry was purchased from Addgene (catalog #44362-AAV2). All chemicals were purchased from Sigma-Aldrich, except D-AP5, which was purchased from Cayman Chemical.

In vivo *viral injection*

Mice were anesthetized with intraperitoneal injection of ketamine (50 mg/kg)–xylazine (5 mg/kg) mixture. A 33-gauge injection needle was used to bilaterally inject 1 μl/site (0.33 μl/min) of adeno-associated virus (AAV) solution into the BLA (in millimeters: from bregma, anterior-posterior (AP), −1.10; ML, ±2.95; dorsal-ventral (DV), −5.10), vHip (from lambda, AP, +1.35; ML, ±2.8; DV, −5.05) or VTA (from lambda, AP, +1.40; medial-lateral (ML), ±0.38; DV, −4.6). After surgery, mice were placed on a heating pad for recovery. Carprofen (5 mg/kg) was injected (subcutaneously) daily for up to 3 d after surgery. Mice were kept in their home cages for four to five weeks to allow for viral expression before electrophysiological experiments. In the experiment of chemogenetic manipulation of presynaptic DA terminals, pAAV-hSyn-DIO-hM4Di-mCherry was injected into the VTA of DAT-Cre mice. Mice with no viral injection or injection of AAV-DIO-mCherry were used as controls.

Slice preparation for electrophysiology

To prepare acute brain slices, we decapitated mice under isoflurane anesthesia. Sagittal slices (250 μm) containing the NAc were prepared on a VT1200S vibratome (Leica) in a 4°C cutting solution, containing (in mM) 135 *N*-methyl-D-glucamine, 1 KCl, 1.2 KH_2PO_4, 0.5 $CaCl_2$, 1.5 $MgCl_2$, 20 choline-HCO_3, and 11 glucose, saturated with 95% O_2/5% CO_2, pH adjusted to 7.4 with HCl. Osmolality was adjusted to 300. Slices were incubated in artificial cerebrospinal fluid (aCSF), containing (in mM) 119 NaCl, 2.5 KCl, 2.5 $CaCl_2$, 1.3 $MgCl_2$, 1 NaH_2PO_4, 26.2 $NaHCO_3$, and 11 glucose, with the osmolality adjusted to 290–295, saturated with 95% O_2/5% CO_2. The brain slices were incubated at 34°C for 30 min and then allowed to recover for >30 min at 20–22°C before experimentation.

Optogenetic stimulation

The laser systems for optogenetic stimulation (RLM635TA-400S-FC for 635 nm, BLM445TA-300FC for 445 nm) were purchased from Shanghai Laser & Optics Century Co, Ltd and the 473-nm laser source was purchased from IkeCool. In experiments that require two lasers, a customized 1 × 2 fanout bundle (FG200UCC-FBUNDLE, Thorlabs Inc.) was used to connect both laser sources to a single fluorescence port on the Olympus BX51WI microscope. Laser beams were reflected by a dichroic filter (640FDC4001-C, Knight Optical) and converged by the microscope condenser. The laser beams then passed through a customized cube (Chroma Technology Corp) to reach the objective lens of the microscope. The output power of each laser was separately calibrated before each experiment by a laser power meter (S130A; Thor Labs) below the objective lens. In experiments involving selecting D1 versus D2 MSNs, the excitation light (wavelength at 533–585 nm) used to detect tdTomato signals might introduce interference to the expressed rhodopsins. Hence, in these experiments, we limited the light exposure within <1 s each time for three to five times (>30 s apart), a procedure sufficient to locate a tdTomato-positive versus negative MSN. In pilot experiments, this short exposure evoked synaptic activities but did not induce residual changes in either vH-to-NAcSh or BLA-to-NAcSh synaptic transmission.

Electrophysiological recordings

All recordings were made in the medial NAcSh (AP 1.4 ± 0.1 mm), with the recorded MSNs presumably from both the rostral and caudal subregions, respectively. The rostral and caudal NAcSh exhibit topographically differential innervation from the BLA and vH and differential activities during motivated behaviors (Reed et al., 2018; Castro and Bruchas, 2019). However, limited by our recording condition in mice, we did not intend to make a comparison between the two subregions, but pooled all recorded MSNs together to represent the medial NAcSh. The internal solution filling the electrodes contained (in mM): 130 $KMeSO_3$, 10 KCl, 10 HEPES, 0.4 EGTA (K), 3 Mg-ATP, 0.5 Na_3-GTP, and 7.5 phosphocreatine. In some experiments, Na_3-GTP was replaced with 1 mM GDP-β-S. The series resistance of electrodes was typically 9–20 MΩ, uncompensated, and monitored continuously during recording. Cells with a change in series resistance >20% were excluded from subsequent data collection. Synaptic

currents were recorded with a MultiClamp 700B amplifier, filtered at 2.6–3 kHz, amplified five times, and then digitized at 20 kHz.

In experiments involving activation of both Chrimson and Channelrhodopsin 2 (ChR2), the 635-nm laser at 0.1–0.4 mW was used first to establish stable EPSCs triggered by Chrimson, with the amplitude typically between 100–200 pA. The 635-nm laser was then decreased to a minimal threshold power, which barely induced EPSCs (i.e., 0–20 pA). The 445-nm laser was then used at a power less than or equal to this threshold power. This precautious procedure further minimized the chance of cross contamination between Chrimson-induced and ChR2-induced EPSCs in a single slice setup. In all experiments, the laser pulse duration was set at 1 ms. In recording of EPSCs, GABAergic receptor antagonists were not included. Although previous studies show that action potentials could be triggered in NAc fast-spiking interneurons (FSIs) by optogenetic stimulation of glutamatergic inputs, the laser powers were relatively high (Yu et al., 2017). In the current studies, very low laser powers were employed to minimize cross-projection contamination, reducing the likelihood of triggering action potentials in FSIs. Furthermore, MSNs were recorded at −70 mV, which was close to the reversal potential of GABAergic synapses, further minimizing the potential contribution of GABAergic transmission to our recorded synaptic responses.

The EPSC rise time was defined as the time that the EPSC rose from 10% of its peak amplitude to the peak. The EPSC decay time was defined as the time that the EPSC decay declined from its peak to 37% of its peak value. The PPR was measured for each two-pulse train and then averaged across all trains.

Data acquisition and statistics

All results are shown as mean ± SEM. Most experiments were replicated in 4–16 mice. All data collection was randomized. All data were assumed to be normally distributed. No statistical methods were used to predetermine sample sizes, but our sample sizes were similar to those reported in previous publications with similar experimental designs (Wang et al., 2018; Wright et al., 2020; Xia et al., 2020; Ge et al., 2021). All data were analyzed offline, and investigators were not blinded to experimental conditions during the analyses.

To detect the induction of LTP, one-way ANOVA repeated measures was used to compare the EPSC amplitudes before and after Sync stimulation. The mean EPSC amplitudes were calculated by averaging all EPSCs over the time segment of 5 min for each condition. To compare the LTP magnitude, the mean amplitudes of EPSCs over the last 5-min period of recording after Sync were used for comparison.

A total of 242 mice were used for this study, among which 67 mice were excluded from the final data analysis because of the following reasons: (1) four mice were excluded because of health issues after surgeries (e.g., >20% drop in body weight in a day); (2) 55 mice were excluded because of off-target stereotaxic injections or poor viral expression; and (3) eight mice were excluded because of experimental failures (e.g., unsuccessful slice preparations, failed recordings, or other experimental incidents). No animals were excluded after data acquisition was accomplished. Data from male and female mice were compared whenever possible but as no trend toward difference (i.e., $p < 0.1$) was detected for any key endpoints, they were combined. Repeated experiments for the same group were pooled together for statistical analysis. For all datasets, the sample sizes are presented as the number of recordings. Number of animals were presented in the figure legends. Statistical significance was assessed using paired or unpaired *t* tests, or one-way or two-way ANOVA followed by Bonferroni *post hoc* test, as specified in the related text. Two-tailed tests were performed for all analyses, and statistical significance was set at $p < 0.05$. Statistical analyses were performed in GraphPad Prism (v7) and SPSS v19 (IBM).

Results

Dual-rhodopsin system

To evoke both the vH-to-NAcSh and BLA-to-NAcSh transmissions to the same MSNs, we optimized a dual-rhodopsin optogenetic system, involving viral expression of ChR2 and Chrimson, which are preferentially activated by lights with different wavelengths (Klapoetke et al., 2014; Fig. 1*A*). We first determined the laser parameters that could selectively activate ChR2-expressing versus Chrimson-expressing presynaptic fibers without cross-contamination. Specifically, we injected AAV-ChR2-EYFP or AAV-Chrimson-tdTomato into one of the two NAcSh projecting regions. Five to eight weeks later, we prepared the NAc brain slices, in which EYFP or tdTomato signals were detected in presynaptic fibers, indicating the expression of ChR2 or Chrimson, respectively. Using whole-cell voltage-clamp recording, we measured synaptic currents in NAcSh MSNs evoked by laser stimulation (pulse duration, 1 ms); lasers at the wavelength of 445, 473, or 635 nm were sequentially applied (Fig. 1*B*). For ChR2-expressing presynaptic fibers, both 445- and 473-nm lasers, but not the 635-nm laser, evoked synaptic responses in NAcSh MSNs (Fig. 1*C–E*). Notably, the 635-nm (red) laser at ≤0.5 mW activated Chrimson (see below) but did not trigger ChR2-evoked synaptic responses, and thus could be used for Chrimson-selective stimulation. For Chrimson-expressing presynaptic fibers, both the 473- and 635-nm lasers evoked synaptic responses with the 635-nm laser exhibiting higher efficacies. The 445-nm laser did not evoke synaptic responses when the laser power was set at 0.5 mW or lower (Fig. 1*F–H*). As such, the 445 nm (purple) laser at ≤0.2 mW was used for ChR2-selective stimulation under our experimental condition. These optogenetically evoked synaptic responses exhibited fast onset, activation, and decay (see Fig. 1*MN*), and, in similar prior studies, could be inhibited by glutamate receptor-selective antagonists, consistent with EPSCs (Lee et al., 2013; Ma et al., 2014; Xia et al., 2020). We thus used this dual-rhodopsin system to evoke EPSCs selectively from vH-to-NAcSh versus BLA-to-NAcSh synapses in the following experiments.

We expressed bilaterally ChR2 and Chrimson in the vH and BLA, respectively, in the same mice, and evoked EPSCs in MSNs receiving convergent vH-to-NAcSh and BLA-to-NAcSh projections (Fig. 1*I*). We designed a continuous stimulation protocol (~20 min), in which the purple versus red lasers (pulse duration 1 ms) were alternatingly applied, separated by 7.5 s, such that each projection was stimulated every 15 s (Fig. 1*J*). In mice in which the expression of both ChR2 and Chrimson was sufficient, we could evoke EPSCs from both projections in most recorded NAcSh MSNs. When stimulation was applied to each projection in a paired-pulse fashion (interpulse interval 50 ms), EPSCs from both vH-to-NAcSh and BLA-to-NAcSh synapses exhibited a wide range of paired pulse ratios (PPRs; quantified as the ratio of the amplitude of the second EPSC over the amplitude of the first EPSC), suggesting that the basal probability of presynaptic release (Pr) and transmission efficacy vary substantially among synapses in each projection (Fig. 1*K*,*L*). In the same MSNs, the mean PPR of vH-to-NAcSh synapses was lower than BLA-to-NAcSh synapses (vH, 1.2 ± 0.1; BLA, 1.7 ± 0.1; $n = 37$ from 21 mice, $p < 0.01$, paired *t* test; Fig. 1*L*), which may be because of an overall higher Pr in vH-to-NAcSh transmission or slightly different properties of ChR2-mediated versus Chrimson-mediated presynaptic activation (Z. Liu et al., 2016).

In the same MSNs, when the EPSCs from both projections were scaled and aligned to their peak amplitudes, they exhibited similar rise and decay kinetics consistent with fast glutamatergic transmission (in ms: rise, vH 2.1 ± 0.1, BLA 2.1 ± 0.1, $p = 0.69$; decay, vH 3.9 ± 0.1, BLA 4.0 ± 0.1, $p = 0.37$; $n = 22$ from 17 mice, paired *t* test; Fig. 1*M*,*N*). The similar EPSC kinetics also suggested that, within the same

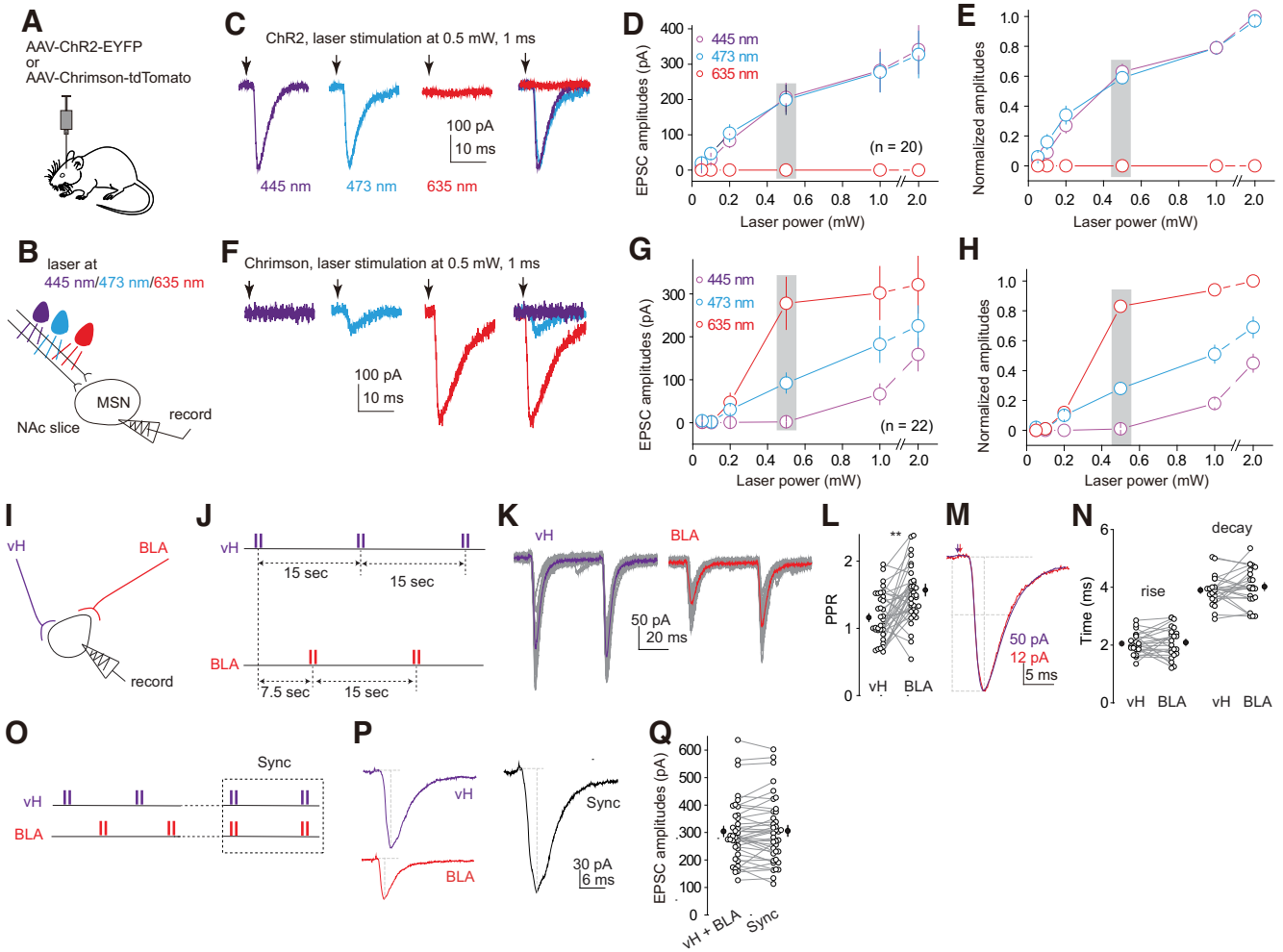

Figure 1. Electrophysiological separation of vH-to-NAcSh and BLA-to-NAcSh projections with the Dual-rhodopsin system. ***A***, Diagram showing injection of a single AAV, either AAV-ChR2-EYFP or AAV-Chrimson-tdTomato, in a single NAcSh-projecting brain region. ***B***, Diagram showing the experimental setup, in which EPSCs were recorded from NAcSh MSNs in response to optogenetic stimulation of single rhodopsin-expressing presynaptic fibers by sequential application of lasers of three different wavelengths. ***C***, Example EPSCs evoked in the same MSN by optogenetic stimulation of ChR2-expressing presynaptic fibers with 445-, 473-, or 635-nm laser. ***D***, Summary of the amplitudes of ChR2-evoked EPSCs by 445-, 473-, and 635-nm lasers at different powers. ***E***, Summary of the same results in ***D*** after normalizing the amplitudes of EPSCs to those evoked by the 445-nm laser at 2 mW. ***F***, Example EPSCs evoked by optogenetic stimulation of Chrimson-expressing presynaptic fibers with 445-, 473-, or 635-nm laser. ***G***, Summary of the amplitudes of Chrimson-evoked EPSCs by 445-, 473-, and 635-nm lasers at different powers. ***H***, Summary of the same results in ***G*** after normalizing the amplitudes of EPSCs to those evoked by the 635-nm laser at 2 mW. ***I***, Diagram showing recording of the same MSN in response to optogenetic stimulation of vH-to-NAcSh versus BLA-to-NAcSh projections. ***J***, Schematics of the alternating stimulation protocol, in which the ChR2-expressing vH projection and Chrimson-expressing BLA projection were alternatingly stimulated with a two-pulse train: interpulse interval, 50 ms; train interval within each projection, 15 s; train interval between the two projections, 7.5 s. ***K***, EPSCs induced by the alternating stimulation protocol in an example MSN (colored traces depict the average of individual gray traces). ***L***, Summary showing a higher mean PPR at BLA-to-NAcSh synapses compared with vH-to-NAcSh synapses. ***M***, Example EPSCs from vH-to-NAcSh and BLA-to-NAcSh synapses scaled and aligned at their peaks. ***N***, Summary showing similar rise and decay kinetics of EPSCs from vH-to-NAcSh versus BLA-to-NAcSh synapses. ***O***, Schematics of Sync protocol, in which the application of 445- and 635-nm lasers was synchronized over 2 min (15 s apart) after the alternating stimulation procedure. ***P***, Example EPSCs evoked by alternating stimulation of vH-to-NAcSh and BLA-to-NAcSh projections and by Sync stimulation. ***Q***, Summary showing that summed amplitudes of vH-to-NAcSh and BLA-to-NAcSh EPSCs in individual MSNs were similar to the amplitudes of Sync-evoked EPSCs. $^{**}p < 0.01$

MSNs, vH-to-NAcSh and BLA-to-NAcSh synapses share similar dendritic filtering conditions. We then adjusted the stimulation protocol such that after a period of alternating stimulations, stimulations of the two projections were synchronized (Sync; stimulation intensities remained constant), creating a time-locked co-activation (Fig. 1*O*). In the same MSNs, the amplitude of Sync-induced EPSCs was equal to the algebraic summation of the amplitudes of EPSCs evoked separately from vH-to-NAcSh and BLA-to-NAcSh synapses (in pA: vH + BLA, 304.1 ± 19.1; Sync, 306.0 ± 20.2, $n = 37$ from 21 mice, $p = 0.77$, paired t test; Fig. 1*P*,*Q*). Such a lack of nonlinear summation is common among synapses within the limbic inputs to the NAcSh, reflecting minimal direct electrical interaction between the two projections (Xia et al., 2020).

Sync-induced LTP at vH-to-NAcSh synapses

In cue-conditioned motivated behaviors, vH and BLA neurons are activated with a similar time course, resulting in potential time-locked co-activation of vH-to-NAcSh and BLA-to-NAcSh synapses (Albertin and Wiener, 2015; Lansink et al., 2016; Grewe et al., 2017; Jarzebowski et al., 2022). To determine the cellular consequences of this time-locked co-activation, we started the alternating stimulation protocol to first establish baselines for EPSCs evoked from both vH-to-NAcSh and BLA-to-NAcSh synapses, then applied the Sync stimulation to the two projections eight times over 2 min and returned to alternating stimulation trials (Fig. 2*A*). Thus, EPSCs from each projection were sampled before, during, and after Sync.

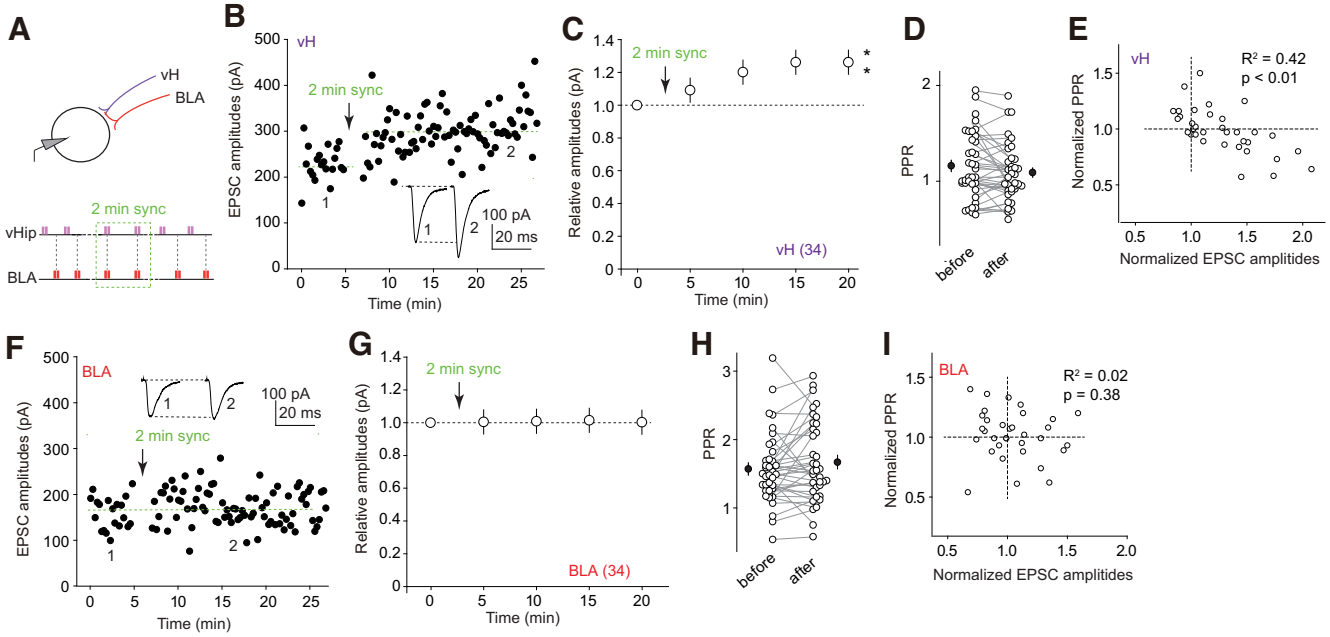

Figure 2. Sync-induced heterosynaptic LTP at vH-to-NAcSh synapses. ***A***, Experimental schematics for inducing Sync-induced LTP. ***B***, ***F***, Trials of amplitudes of EPSCs from vH-to-NAcSh (***B***) and BLA-to-NAcSh (***F***) synapses in an example MSN before and after Sync. ***C***, ***G***, Summaries showing that Sync stimulation of vH-to-NAcSh and BLA-to-NAcSh projections selectively induced LTP at vH-to-NAcSh (***C***), but not BLA-to-NAcSh, synapses (***G***). ***D***, ***H***, Summaries showing that Sync did not change the mean PPR at vH-to-NAcSh (***D***) or BLA-to-NAcSh (***H***) synapses. ***E***, ***I***, Summaries showing that the normalized PPRs are negatively correlated to the normalized amplitudes of EPSCs from vH-to-NAcSh (***E***), but not BLA-to-NAcSh (***I***), synapses after Sync. $^{**}p < 0.01$

Sync induced a persistent increase in the amplitudes of EPSCs from vH-to-NAcSh synapses, an LTP phenomenon ($F_{(4,132)}$ = 17.6, $p < 0.01$, $n = 34$ from 19 mice, one-way ANOVA repeated measures followed by Bonferroni *post hoc* test; Fig. 2*B*,*C*). In parallel, we also measured the PPR in each MSN. The averaged PPR across all recorded MSNs was similar before versus after Sync ($p = 0.09$, paired *t* test; Fig. 2*D*). However, we noticed the high variability of PPR among individual MSNs (Figs. 1*L*, 2*D*,*H*). The variable data created an opportunity for correlational analysis. When the normalized EPSC amplitude after Sync was plotted against the normalized PPR ($PPR_{after\ Sync}/PPR_{before\ Sync}$) in each MSN, a negative correlation was detected (R^2 = 0.42, $p < 0.01$; Fig. 2*E*). Thus, a potential increase in the Pr of presynaptic release was linked to the expression magnitude of this LTP. In contrast to vH EPSCs, Sync did not induce detectable changes in BLA EPSCs ($F_{(4,132)}$ = 1.1, $p = 0.34$, $n = 34$ from 19 mice, one-way ANOVA repeated measures followed by Bonferroni *post hoc* test), or their PPRs ($p = 0.18$, paired *t* test; R^2 = 0.02, $p = 0.38$; Fig. 2*F*–*I*). Taken together, a brief time-locked co-activation of the vH and BLA projections selectively induced LTP at vH-to-NAcSh synapses.

It is worth noting that the lack of heterosynaptic plasticity at BLA-to-NAcSh synapses is not likely to result from the potentially different properties of Chrimson-mediated presynaptic depolarization. In our parallel studies, a 20-Hz stimulation of Chrimson-expressing BLA presynaptic fibers induces monosynaptic LTP at BLA-to-NAcSh synapses (Xia et al., 2020).

LTP in D1 and D2 MSNs

MSNs that preferentially express dopamine D1 receptors versus D2 receptors comprise the two major neuronal populations in the NAc (Gong et al., 2003; Gerfen and Surmeier, 2011). D1 and D2 MSNs are coupled with different intracellular signaling pathways in response to dopamine and imbedded in different neural circuits that regulate motivated behavior (Allichon et al., 2021; Zinsmaier et al., 2022). To determine whether this Sync-induced LTP was D1 or D2 MSN-specific, we employed a mouse line in which D1 MSNs are genetically tagged with tdTomato (Shuen et al., 2008; Ade et al., 2011). Extensive prior studies demonstrate that, in brain slices, the presence versus absence of tdTomato fluorescence reliably predicts D1 versus D2 MSNs (Shuen et al., 2008; Ade et al., 2011; Lobo et al., 2013; Graziane et al., 2016). This identification method was thus used here to operationally define these two neuronal types.

In D1-tdTomato mice, we expressed ChR2 and Chrimson in the vH and BLA, respectively. For a direct comparison of D1 versus D2 MSNs, in each experiment, we performed dual-recording to simultaneously record a tdTomato -positive MSN and an adjacent tdTomato-negative MSN, in response to optogenetic stimulation of the vH-to-NAcSh and BLA-to-NAcSh projections (Fig. 3*A*). Optogenetic stimulation of either vH-to-NAcSh or BLA-to-NAcSh projection evoked EPSCs in both simultaneously recorded D1 and D2 MSNs (Fig. 3*B*). Furthermore, the amplitudes of EPSCs were comparable between vH-to-D1 versus vH-to-D2 synapses, as well as between BLA-to-D1 versus BLA-to-D2 synapses (in pA: vH-D1 169.7 ± 18.6, vH-D2 215.0 ± 18.6, $p = 0.07$; BLA-D1 154.2 ± 21.3, BLA-D2 126.3 ± 17.5, $p = 0.38$; paired *t* test, $n = 27$ pairs from 21 mice; Fig. 3*C*), suggesting overall unbiased intraprojection innervation of D1 versus D2 MSNs. We did not intend to compare the innervation intensity between vH-to-NAcSh and BLA-to-NAcSh projections, because of the lack of approaches that could calibrate the presynaptic activation levels between the two projections.

After establishing stable baselines over the alternating stimulation protocol, we applied the 2-min Sync protocol (Fig. 3*D*), which simultaneously induced LTP at both vH-to-D1 and vH-to-D2 synapses ($F_{(2,52)}$ = 17.5, $p < 0.01$, two-way ANOVA with repeated measures; $p < 0.01$ before versus after Sync for both D1 and D2, Bonferroni *post hoc* test), but not at BLA-to-D1 or BLA-

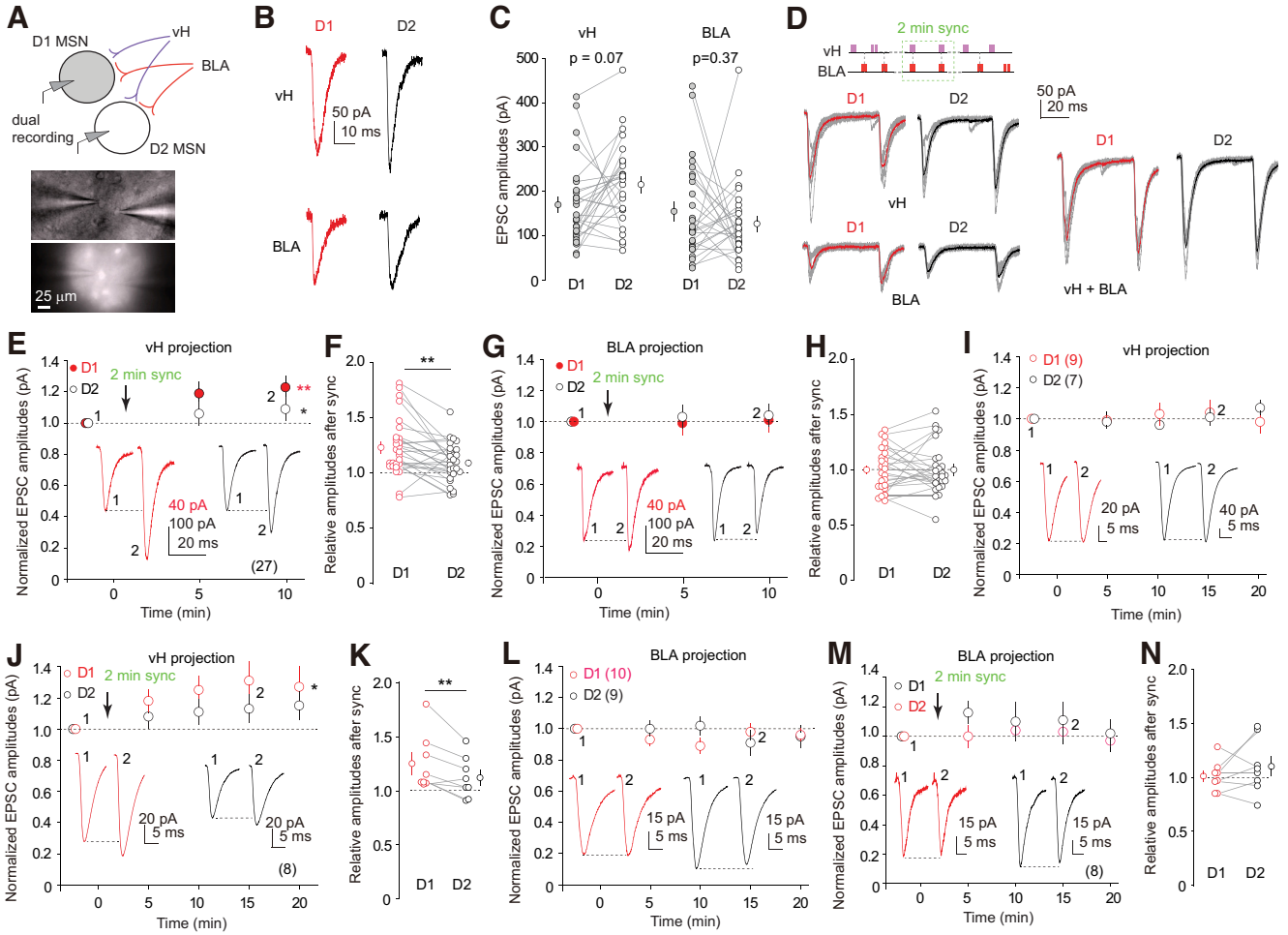

Figure 3. Sync LTP differed in D1 and D2 MSNs. ***A***, Diagram showing the dual-recording, dual-rhodopsin experimental setup, in which a D1 and a putative D2 MSN were simultaneously recorded in response to optogenetic stimulation of vH-to-NAcSh and BLA-to-NAcSh projections. Inset, Example image showing dual recording of tdTomato-positive (D1) and tdTomato-negative (D2) MSNs. ***B***, Example EPSCs in dual-recorded D1 and D2 MSNs evoked by optogenetic stimulation of vH-to-NAcSh and BLA-to-NAcSh projections. ***C***, Summaries showing similar amplitudes of EPSCs in dual-recorded D1 and D2 MSNs evoked by stimulation of either vH-to-NAcSh or BLA-to-NAcSh projections. ***D***, Example EPSCs in dual-recorded D1 and D2 MSNs evoked before and during Sync (stimulation schematics shown in upper panel). ***E***, ***G***, Summaries showing that Sync stimulation of vH and BLA projections induced LTP at both vH-to-D1 and vH-to-D2 synapses (***E***) without changing the amplitudes of EPSCs from BLA-to-D1 or D2 synapses (***G***). ***F***, ***H***, Summaries showing that, after Sync, the relative amplitudes of EPSCs from vH-to-D1 synapses were higher than vH-to-D2 synapses (***F***), while the amplitudes of EPSCs from BLA-to-D1 and BLA-to-D2 synapses were similar after Sync (***H***). ***I–N***, Summaries showing in two parallel experiments performed in tandem that EPSCs evoked from vH- (***I***) and BLA-to-D1 and D2 synapses (***L***) remained constant over the 25-min recording without Sync, while Sync stimulation induced LTP at both vH-to-D1 and vH-to-D2 synapses (***J***) with higher magnitude at vH-to-D1 synapses (***K***), and Sync stimulation did not affect BLA-to-D1 or BLA-to-D2 synaptic transmission (***M***) or relative strengths between these synapses (***N***). $*p < 0.05$; $**P < 0.01$

to-D2 synapses ($F_{(2,52)} = 0.32$, $p = 0.70$, two-way ANOVA; $p = 0.45$, D1 versus D2 after Sync, paired t test; Fig. 3*D–H*). However, compared with vH-to-D2 synapses, the magnitude of LTP at vH-to-D1 synapses was higher, indicating a D1 MSN-biased feature of this LTP ($p < 0.01$, paired t test; Fig. 3*F*).

To address whether the time-locked activation was essential for the induction of this LTP, we used the same procedure but recorded EPSCs from only one projection without Sync. Without Sync, neither vH-to-D1/2 nor BLA-to-D1/2 synapses exhibited potentiation (vH, $F_{(4,56)} = 0.4$, $p = 0.40$; BLA, $F_{(4,56)} = 0.4$, $p = 0.80$, two-way ANOVA repeated measures), while in the interleaved controls, in which Sync was applied, vH-to-D1 and vH-to-D2 synapses exhibited LTP (vH, $F_{(4,28)} = 3.9$, $p = 0.01$; BLA, $F_{(4,28)} = 1.1$, $p = 0.40$, two-way ANOVA repeated measures; $p < 0.01$ before versus after Sync for both vH-D1 and vH-D2, Bonferroni *post hoc* test), with D1 MSNs exhibiting higher LTP magnitude compared with D2 MSNs ($p = 0.01$, paired t test; Fig. 3*I–N*). Thus, LTP induction at vH-to-NAcSh synapses required the simultaneous activation of BLA inputs, indicating this LTP is heterosynaptically induced.

Dopamine signaling

To determine the cellular mechanisms that were activated to induce this LTP, we first examined NMDA receptors (NMDARs), well-known coincidence detectors that mediate the induction of several forms of LTP at glutamatergic synapses. However, including the NMDAR-selective antagonist D-AP5 (50 μM) in the recording bath did not prevent Sync-induced LTP at either vH-to-D1 or vH-to-D2 synapses, and did not induce changes at BLA-to-D1 or BLA-to-D2 synapses (vH, $F_{(4,76)} = 11.6$, $p < 0.01$; BLA, $F_{(4,76)} = 2.3$, $p = 0.07$; $p < 0.01$ before versus after Sync for both vH-D1 and vH-D2; Bonferroni *post hoc* test; Fig. 4*A*,*B*). We next examined $GABA_A$ receptor ($GABA_AR$)-mediated transmission, which is involved in several forms of heterosynaptic plasticity (Chevaleyre and Castillo, 2004; Q.S. Liu et al., 2005). Including the $GABA_AR$-selective antagonist picrotoxin (100 μM) in the recording

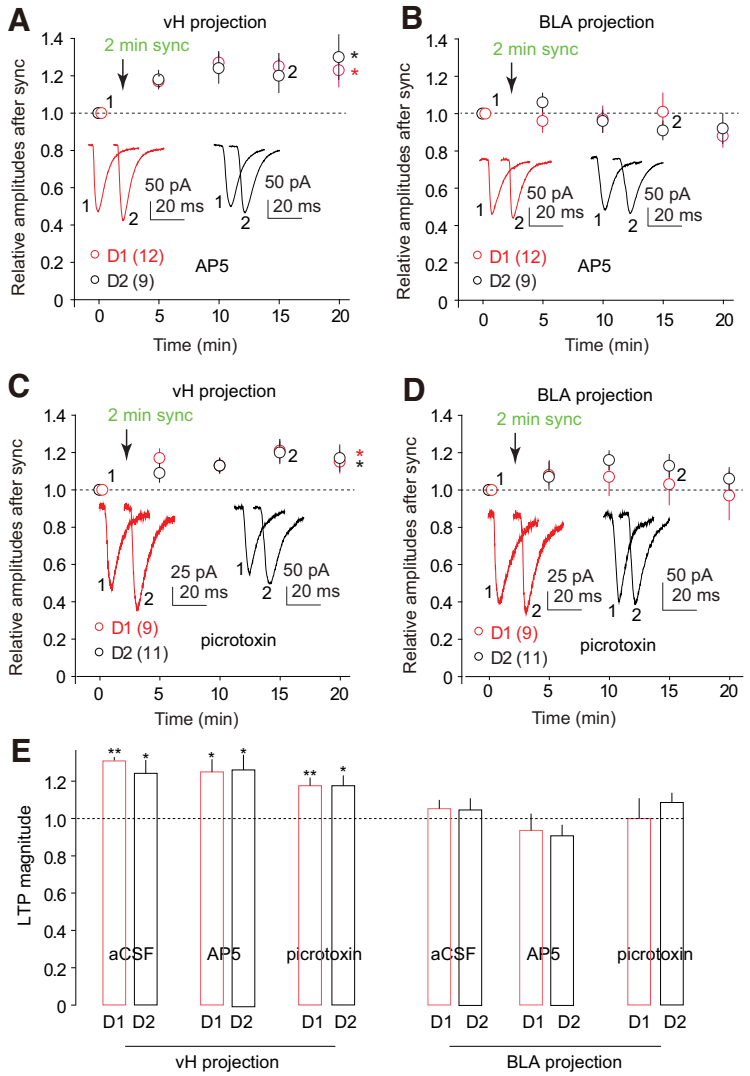

Figure 4. Inhibition of NMDA or $GABA_A$ receptors did not prevent Sync-induced heterosynaptic LTP. ***A***, ***B***, Summaries showing that, in the presence of D-AP5, Sync-induced LTP was intact at both vH-to-D1 and vH-to-D2 synapses (***A***) and remained absent at BLA-to-D1 and BLA-to-D2 synapses (***B***). ***C***, ***D***, Summaries showing that, in the presence of picrotoxin, Sync-induced LTP was intact at vH-to-D1 and vH-to-D2 synapses (***C***) and remained absent at BLA-to-D1 and BLA-to-D2 synapses (***D***). ***E***, Summary of the LTP magnitude in each experimental condition. The LTP magnitude was represented as the ratio of the amplitude of EPSCs during 11–20 min after Sync over the amplitude of EPSCs during the 5-min recording before Sync. Data statistical results are combined from all related recordings in this and previous figures. $^*p < 0.05$; $^{**}p < 0.01$.

bath also did not prevent Sync-induced LTP at vH-to-D1 or vH-to-D2 synapses (vH, $F_{(4,76)} = 9.1$, $p < 0.01$; BLA, $F_{(4,76)} = 2.1$, $p = 0.10$, two-way ANOVA; $p < 0.05$ before versus after Sync for vH-D1 and vH-D2, Bonferroni *post hoc* test; Fig. 4*C–E*). It is worth noting it appeared that the difference in LTP magnitudes between vH-to-D1 versus vH-to-D2 synapses was neutralized in the presence of D-AP5 or picrotoxin (Fig. 4*A*,*C*). Despite these effects, the results ruled out NMDARs and $GABA_A$Rs in the induction of this Sync-induced heterosynaptic LTP.

Projecting from the ventral tegmental area (VTA), dopaminergic fibers in the NAcSh form synapses around glutamatergic synapses on MSN dendrites, regulating synaptic transmission both presynaptically and postsynaptically (Sesack and Grace, 2010; Tritsch and Sabatini, 2012). Targeting dopamine (DA) signaling, we included either the D1 receptor-selective antagonist SCH23390 (1 μM) or the D2 receptor-selective antagonist eticlopride (0.1 μM) in the recording bath. SCH23390, but not eticlopride, prevented Syn-induced LTP at both vH-to-D1 and vH-to-D2 synapses, and neither of these antagonists affected BLA-to-D1 or BLA-to-D2 synaptic transmission (SCH-vH, $F_{(3,21)} = 1.5$, $p = 0.24$; SCH-BLA, $F_{(3,21)} = 0.8$, $p = 0.48$; eti-vH, $F_{(3,15)} = 15.7$, $p < 0.01$; eti-BLA, $F_{(3,15)} = 1.1$, $p = 0.37$, two-way ANOVA repeated measures; $p < 0.01$ before versus after Sync for both vH-eti-D1 and vH-eti-D2; Fig. 5*A–D*). Thus, the D1 receptor-coupled signaling is an essential component within the heterosynaptic mechanism that mediates the induction of this heterosynaptic LTP.

D1 receptors are G-protein-coupled receptors expressed at both presynaptic and postsynaptic terminals as well as glial cells (Tritsch and Sabatini, 2012). The higher LTP magnitude in D1 over D2 MSNs (Fig. 3*F*) prompted us to test whether the postsynaptic D1 receptors were essential for LTP induction. In the recording electrode, we included guanosine 5'-*O*-2-thiodiphosphate (GDP-β-S; 1 mM), which antagonizes G-protein signaling. While the same GDP-β-S-based approach disrupts postsynaptic D1 or D2 receptor-mediated synaptic modulation (Maguire and Werblin, 1994; Nisenbaum et al., 1998; Schoffelmeer et al., 2000; Nimitvilai et al., 2017), it did not prevent Sync-induced LTP at vH-to-D1 or vH-to-D2 synapses, and did not affect BLA-to-D1/2 synaptic transmission (vH, $F_{(3,33)} = 7.8$, $p < 0.01$; BLA, $F_{(3,33)} = 2.0$, $p = 0.14$, two-way ANOVA repeated measures; $p < 0.01$ before versus after Sync for both vH-D1 and vH-D2; Fig. 5*E*,*F*). These results do not support an involvement of postsynaptic D1 receptors, leaving the possibility that presynaptic or non-MSN expressed D1 receptors contribute to the induction mechanism.

Lacking rhodopsin expression, VTA-to-NAcSh dopaminergic fibers were not likely to be activated directly by Sync stimulation. As such, a lingering question is whether the above effects of D1-coupled signaling were initiated by DA released from dopaminergic fibers. To address this, we employed DAT-Cre mice and selectively expressed an inhibitory DREADD (hM4Di) in VTA DA neurons in addition to the dual-rhodopsin expression. During recording, we superfused the NAc slices with CNO (10 μM) to attenuate the potential activation of dopaminergic fibers. Under this condition, vH-to-NAcSh synapses failed to develop Sync-induced LTP, and BLA-to-NAcSh synaptic transmission was not affected (vH-hM4D, $F_{(3,33)} = 0.2$, $p = 0.90$; vH-control, $F_{(3,39)} = 7.7$, $p < 0.01$; BLA-hM4Di, $F_{(3,33)} = 1.1$, $p = 0.37$; BLA-hM4Di, $F_{(3,33)} = 0.6$, $p = 0.60$, two-way ANOVA repeated measures; Fig. 6*A*,*B*). Thus, possibly through local circuits or non-neuronal cells, co-activation of vH-to-NAcSh and BLA-to-NAcSh projections indirectly activated adjacent dopaminergic terminals, and the resulting activation of D1 receptors provided a permissive condition for the induction of this heterosynaptic LTP (Fig. 6*C*,*D*).

Discussion

Using a dual-rhodopsin system, we demonstrated a heterosynaptic LTP at vH-to-NAcSh synapses induced by time-locked

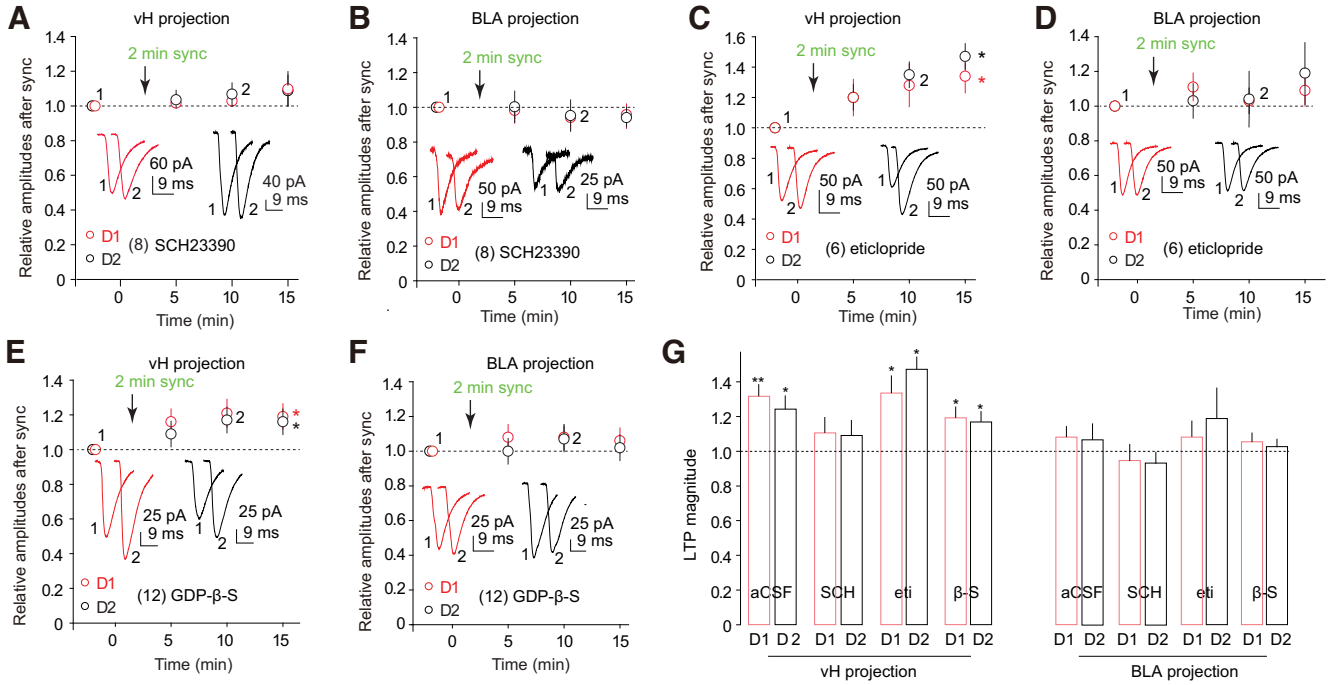

Figure 5. DA D1 receptor-coupled signaling was essential for Sync-induced LTP. ***A***, ***B***, Summaries showing that, in the presence of SCH23390, Sync-induced LTP was prevented at vH-to-D1 and vH-to-D2 synapses (***A***) and remained absent at BLA-to-D1 and BLA-to-D2 synapses (***B***). ***C***, ***D***, Summaries showing that, in the presence of eticlopride, Sync-induced LTP was intact at vH-to-D1 and vH-to-D2 synapses (***C***) and remained absent at BLA-to-D1 and BLA-to-D2 synapses (***D***). ***E***, ***F***, Summaries showing that, with GDP-β-S perfused in MSNs, Sync-induced LTP was intact at vH-to-D1 and vH-to-D2 synapses (***E***) and remained absent at BLA-to-D1 and BLA-to-D2 synapses (***F***). ***G***, Summary of the LTP magnitude in each experimental condition. The LTP magnitude was represented as the ratio of the amplitude of EPSCs after the Sync induction over the amplitude of EPSCs before Sync. Data and statistical results are combined from all related recordings in this and previous figures. $^{*}p < 0.05$; $^{**}p < 0.01$.

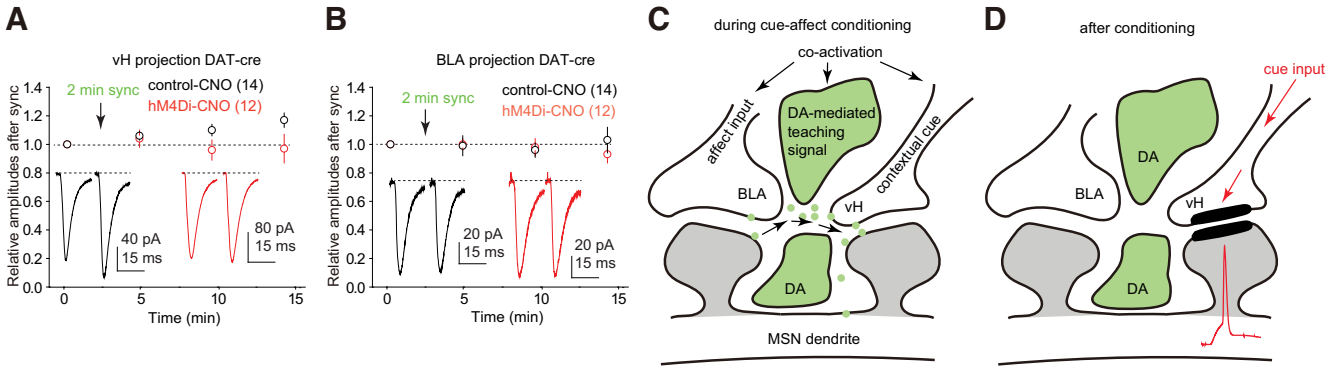

Figure 6. Chemogenetic inhibition of DA presynaptic terminals in the NAcSh prevented Sync-induced LTP. ***A***, Perfusion of CNO prevented the induction of Sync-induced LTP at vH-to-NAcSh synapses in slices in which presynaptic DA terminals selectively expressed hM4Di, but not in control slices. ***B***, Perfusion of CNO did not affect BLA-to-NAcSh synaptic transmission before or after Sync stimulation in slices with or without hM4Di expression in presynaptic DA terminals. ***C***, ***D***, Diagrams illustrating the hypothesis that during cue-affect conditioning, co-activation of the cue-encoding vH and affect-encoding BLA projections together with a DA-mediated "teaching signal" create a heterosynaptic condition (***C***) to induced LTP at vH-to-NAcSh synapses. Through this LTP, the conditioned cue encoded by the vH projection gains increased power to excite NAcSh MSNs (***D***).

co-activation of BLA-to-NAcSh projections. This LTP may serve a circuit mechanism through which cue-encoding inputs temporally contingent with arousing inputs acquire increased power to excite NAcSh MSNs and promote cue-conditioned reinforcement.

Heterosynaptic interaction/plasticity

The similar EPSC kinetics suggest that vH-to-NAcSh and BLA-to-NAcSh synapses reside on similar dendritic locations (Fig. 1*M*,*N*). Indeed, most limbic projections form synapses on the same dendritic segments of NAcSh MSNs, and on many occasions, these synapses are organized into clusters (French and Totterdell, 2002, 2003; Xia et al., 2020). These anatomic alignments facilitate both dendritic summation and heterosynaptic plasticity.

Few axo-axonic synapses or double-headed spines are observed in the NAc, predicting that most axospinous synapses are self-confined, each encoding unconvoluted information (Xia et al., 2020). Echoing this prediction, EPSCs from vH-to-NAcSh and BLA-to-NAcSh synapses did not exhibit nonalgebraic summation (Fig. 1*P*,*Q*). Through algebraic summation, two subthreshold vH and BLA inputs can be integrated as a suprathreshold drive for NAcSh MSNs. Consistent with this viewpoint, co-stimulation of the hippocampal and BLA projections produces a

synergistic effect on evoking action potentials in NAc MSNs (O'Donnell and Grace, 1995; Mulder et al., 1998).

Beyond the transient effect, our results show that long-term plasticity could be induced heterosynaptically at vH-to-NAcSh synapses. Unlike monosynaptic plasticity at vH-to-NAc synapses induced by sole activation of the same synapses (Dong et al., 2007; Ji et al., 2015; LeGates et al., 2018), Sync-induced LTP relies on co-activation of other synapses and exhibits several heterosynaptic features that may hold the key to understanding the *in vivo* interaction between vH-to-NAcSh and BLA-to-NAcSh projections. Specifically, Sync involved temporally contingent co-activation of heterosynaptic inputs, recapitulating the commonly observed activation patterns of vH and BLA during cue-conditioned motivated behaviors (Tye et al., 2008; Lansink et al., 2012; Leathers and Olson, 2017; Klee et al., 2021). We speculate that this or similar heterosynaptic plasticity is routinely induced *in vivo* to set/reset the vH-to-NAcSh transmission. Consistently, although LTP/LTD can be induced independently in hippocampus-to-NAc or BLA-to-NAc projections, a successful induction in one input often requires activity from the other (Mulder et al., 1997, 1998; Gill and Grace, 2011; Chong et al., 2022).

Dopamine signaling

It has long been known that dopamine regulates monosynaptic plasticity. This is exemplified in spike timing-dependent synaptic plasticity (STDP) observed in several limbic regions, in which co-incidental DA-signaling either facilitates or polarizes the STDP induction (J.C. Zhang et al., 2009; Xu and Yao, 2010; Ji et al., 2017). By demonstrating the essential role of DA in Sync-induced LTP, our current findings reveal a heterosynaptic basis through which co-incidental DA signals provide a time stamp that tags a specific memory (Wise, 2004).

Midbrain DA axons converge with vH and BLA glutamatergic axons at NAc MSN dendrites (Totterdell and Smith, 1989; Sesack and Pickel, 1990; Johnson et al., 1994), where DA presynaptic terminals reside in the intersynapse spaces or on dendritic shafts between glutamatergic synapses (Pickel et al., 1988; Sesack and Grace, 2010), providing an efficient anatomic alignment for DA to bridge vH and BLA synapses (Fig. 6*C*). Pharmacological inhibition of D1 receptors or chemogenetic inhibition of DA axons prevented the Sync-induced LTP. Below, we discuss several questions related to DA and D1 receptors as key contributors to heterosynaptic signaling.

First, our optogenetic stimulation was confined to rhodopsin-expressing fibers. How were the DA axons co-activated? In anesthetized rats, stimulating BLA neurons increased DA levels in the NAc (Floresco et al., 2001). While this may result from the co-activation of a BLA-to-VTA projection, it might also be mediated by glutamatergic receptors on DA nerve terminals (Gracy and Pickel, 1996; Sesack et al., 2003) or local circuits within the NAc. Specifically, cholinergic interneurons (ChNs) within the striatum (including NAc) receive the same cortical/subcortical glutamatergic projections that drive MSN activation (Zhou et al., 2003; Guo et al., 2015; Hirose et al., 2021). ChN-released acetylcholine activates nicotinic receptors on presynaptic DA terminals, evoking DA release (C. Liu et al., 2022). Through this ChN-based local circuit, it is possible that Sync activation of vH/BLA terminals simultaneously increased ChN firing, providing the time-locked DA signal.

Second, if not postsynaptically (Fig. 5), where were the D1 receptors that provided heterosynaptic signaling? In addition to postsynaptic location, D1 receptors are also expressed presynaptically on glutamatergic terminals and axonal varicosities (Levey et al., 1993; Caillé et al., 1996; Naha et al., 2009), as well as on astroglia (Vermeulen et al., 1994; Zanassi et al., 1999; Miyazaki et al., 2004; Nagatomo et al., 2017). In NAc slices, DA or D1 receptor-selective agonists, or optogenetic stimulation of DA terminals, decreases synaptic release Pr, indicating a presynaptic impact of D1 receptors (Nicola et al., 1996; Nicola and Malenka, 1997; L. Zhang et al., 2014; Yu et al., 2019). While this presynaptic impact can be mediated by presynaptic D1 receptors, evidence shows that it can be mediated alternatively through transsynaptic signaling from postsynaptic D1 receptors on MSNs or interneurons (Harvey and Lacey, 1996, 1997; Chergui and Lacey, 1999). Furthermore, activation of D1 receptors on NAc astrocytes induces astrocytic release of ATP/adenosine, which, in turn, depresses synaptic transmission to MSNs through presynaptic A1 receptors (Zanassi et al., 1999; Corkrum et al., 2020). These results demonstrate the presynaptic impact of D1 receptors, although these synapse-inhibitory effects may not directly contribute to the synaptic potentiation in Sync-induced LTP.

Third, D1 receptors play multi-faceted roles in synaptic regulation (Tritsch and Sabatini, 2012). Minutes of agonist perfusion or strong stimulation of dopaminergic terminals may persistently activate D1 receptors at most subcellular locations. Under this condition, the synapse-inhibitory effect dominates. However, when dopamine is introduced focally to activated glutamatergic synapses on striatal MSNs within a 0.3–2 s time window, a cAMP-PKA signaling-dependent synapse-enhancing effect emerges (Yagishita et al., 2014; Kasai et al., 2021). In slices, inhibition of D1 receptors or disruption of DA inputs prevents the LTP induction in NAc or striatal MSNs (Centonze et al., 1999; Calabresi et al., 2000; Kerr and Wickens, 2001; Picconi et al., 2003; Kung et al., 2007; Akopian et al., 2008; Pawlak and Kerr, 2008; Schotanus and Chergui, 2008; Shen et al., 2008; Dallérac et al., 2011; but see LeGates et al., 2018), highlighting the synapse-enhancing impact of D1 receptor-coupled signaling. Thus, activation of D1 receptors can either decrease or increase the efficacy of glutamatergic synaptic transmission, depending on their subcellular locations, interacting partners and activation intensities/durations. For the Sync-induced LTP, we speculate that when activated vH synapses meet the focal and temporally contingent DA signals, the persistent synapse-enhancing effect predominates.

Circuit and behavioral implications

Increasing evidence suggests that NAc MSNs are organized into different neuronal ensembles, each encoding a specific aspect of behavior (Pennartz et al., 1994; Robinson and Carelli, 2008; Warren et al., 2017; Wright and Dong, 2021). The Sync-induced LTP may serve a circuit mechanism for the formation of NAc ensembles. Glutamatergic projections drive the activation of NAc MSNs, and MSNs are more effectively activated when multiple glutamatergic projections are activated simultaneously (O'Donnell and Grace, 1995; Sesack and Grace, 2010). The demonstration of hippocampal place cells and contextual cue-specific engrams/ensembles indicate that separate vH neuronal populations encode different conditioning cues (Lansink et al., 2012; Josselyn et al., 2015; Moser et al., 2017; Tonegawa et al., 2018; Bladon et al., 2019). Similarly, largely separate BLA neurons are activated during different cue-conditioned motivated behaviors (Redondo et al., 2014; Bocchio et al., 2017; Gründemann et al., 2019). Thus, for a given cue-conditioning process, select populations of vH and BLA neurons and their projections to NAc are co-activated. Through Sync-induced LTP, only the co-activated

vH-to-NAc subprojections acquire increased efficacies and preferentially activate the MSNs that are innervated by this subprojection, thus defining the ensemble neurons. This input-based ensemble recruitment can be particularly important for NAc MSNs, which lack intrinsic pace-making machinery (Wright and Dong, 2021; Zinsmaier et al., 2022).

In cue-conditioned motivated behaviors, the conditioning cue obtains reinforcing power. Despite their interwoven roles, the vH and BLA projections may preferentially transmit cue-associated versus incentive-associated information, respectively. In anesthetized rats, strong, but not weak, stimulation of hippocampal inputs evokes action potentials in NAcSh MSNs, indicating that many vH-to-NAcSh inputs are subthreshold in the basal condition (O'Donnell and Grace, 1995; Mulder et al., 1997). Through Sync-induced LTP, some subthreshold vH inputs that are co-activated with BLA inputs can be tuned to suprathreshold inputs, providing an input-specific circuit mechanism through which the conditioning cue acquires or increases its motivational drive to reinforce a behavior.

It has been proposed that NAc afferents interact to mutually gate information flow to MSNs (O'Donnell and Grace, 1995). Interactions between these afferents can enable contextual representations of affect that support approach/avoidance behavior in an immediate sense. However, if the condition is extreme, such as life-threatening, it would be more effective to avoid the context rather than engaging in another negative encounter. In response to such stimuli with high salience, the Sync-induced LTP enables a long-term instantiation of an emotional state on the given context under the "teaching signal" from the dopamine system. As a result, the next time this context is encountered, it can be actively avoided without the need to again engage the BLA-encoded valence inputs.

References

Ade KK, Wan Y, Chen M, Gloss B, Calakos N (2011) An improved BAC transgenic fluorescent reporter line for sensitive and specific identification of striatonigral medium spiny neurons. Front Syst Neurosci 5:32.

Akopian G, Crawford C, Beal MF, Cappelletti M, Jakowec MW, Petzinger GM, Zheng L, Gheorghe SL, Reichel CM, Chow R, Walsh JP (2008) Decreased striatal dopamine release underlies increased expression of long-term synaptic potentiation at corticostriatal synapses 24 h after 3-nitropropionic-acid-induced chemical hypoxia. J Neurosci 28:9585–9597.

Albertin SV, Wiener SI (2015) Neuronal activity in the nucleus accumbens and hippocampus in rats during formation of seeking behavior in a radial maze. Bull Exp Biol Med 158:405–409.

Allichon MC, Ortiz V, Pousinha P, Andrianarivelo A, Petitbon A, Heck N, Trifilieff P, Barik J, Vanhoutte P (2021) Cell-type-specific adaptions in striatal medium-sized spiny neurons and their roles in behavioral responses to drugs of abuse. Front Synaptic Neurosci 13:799274.

Belujon P, Grace AA (2011) Hippocampus, amygdala, and stress: interacting systems that affect susceptibility to addiction. Ann N Y Acad Sci 1216:114–121.

Bladon JH, Sheehan DJ, De Freitas CS, Howard MW (2019) In a temporally segmented experience hippocampal neurons represent temporally drifting context but not discrete segments. J Neurosci 39:6936–6952.

Bocchio M, Nabavi S, Capogna M (2017) Synaptic plasticity, engrams, and network oscillations in amygdala circuits for storage and retrieval of emotional memories. Neuron 94:731–743.

Britt JP, Benaliouad F, McDevitt RA, Stuber GD, Wise RA, Bonci A (2012) Synaptic and behavioral profile of multiple glutamatergic inputs to the nucleus accumbens. Neuron 76:790–803.

Caillé I, Dumartin B, Bloch B (1996) Ultrastructural localization of D1 dopamine receptor immunoreactivity in rat striatonigral neurons and its relation with dopaminergic innervation. Brain Res 730:17–31.

Calabresi P, Gubellini P, Centonze D, Picconi B, Bernardi G, Chergui K, Svenningsson P, Fienberg AA, Greengard P (2000) Dopamine and cAMP-regulated phosphoprotein 32 kDa controls both striatal long-term depression and long-term potentiation, opposing forms of synaptic plasticity. J Neurosci 20:8443–8451.

Castro DC, Bruchas MR (2019) A motivational and neuropeptidergic hub: anatomical and functional diversity within the nucleus accumbens shell. Neuron 102:529–552.

Centonze D, Gubellini P, Picconi B, Calabresi P, Giacomini P, Bernardi G (1999) Unilateral dopamine denervation blocks corticostriatal LTP. J Neurophysiol 82:3575–3579.

Chergui K, Lacey MG (1999) Modulation by dopamine D1-like receptors of synaptic transmission and NMDA receptors in rat nucleus accumbens is attenuated by the protein kinase C inhibitor Ro 32-0432. Neuropharmacology 38:223–231.

Chevaleyre V, Castillo PE (2004) Endocannabinoid-mediated metaplasticity in the hippocampus. Neuron 43:871–881.

Chong YS, Wong LW, Gaunt J, Lee YJ, Goh CS, Morris RGM, Ch'ng TH, Sajikumar S (2022) Distinct contributions of ventral CA1/amygdala co-activation to the induction and maintenance of synaptic plasticity. Cereb Cortex. Advance online publication. Retrieved March 7, 2022. doi:10.1093/cercor/bhac093.

Corder G, Ahanonu B, Grewe BF, Wang D, Schnitzer MJ, Scherrer G (2019) An amygdalar neural ensemble that encodes the unpleasantness of pain. Science 363:276–281.

Corkrum M, Covelo A, Lines J, Bellocchio L, Pisansky M, Loke K, Quintana R, Rothwell PE, Lujan R, Marsicano G, Martin ED, Thomas MJ, Kofuji P, Araque A (2020) Dopamine-evoked synaptic regulation in the nucleus accumbens requires astrocyte activity. Neuron 105:1036–1047.e5.

Dallérac GM, Vatsavayai SC, Cummings DM, Milnerwood AJ, Peddie CJ, Evans KA, Walters SW, Rezaie P, Hirst MC, Murphy KP (2011) Impaired long-term potentiation in the prefrontal cortex of Huntington's disease mouse models: rescue by D1 dopamine receptor activation. Neurodegener Dis 8:230–239.

Dong Z, Cao J, Xu L (2007) Opiate withdrawal modifies synaptic plasticity in subicular-nucleus accumbens pathway in vivo. Neuroscience 144:845–854.

Floresco SB, Blaha CD, Yang CR, Phillips AG (2001) Dopamine D1 and NMDA receptors mediate potentiation of basolateral amygdala-evoked firing of nucleus accumbens neurons. J Neurosci 21:6370–6376.

French SJ, Totterdell S (2002) Hippocampal and prefrontal cortical inputs monosynaptically converge with individual projection neurons of the nucleus accumbens. J Comp Neurol 446:151–165.

French SJ, Totterdell S (2003) Individual nucleus accumbens-projection neurons receive both basolateral amygdala and ventral subicular afferents in rats. Neuroscience 119:19–31.

Ge F, Mu P, Guo R, Cai L, Liu Z, Dong Y, Huang YH (2021) Chronic sleep fragmentation enhances habenula cholinergic neural activity. Mol Psychiatry 26:941–954.

Gerfen CR, Surmeier DJ (2011) Modulation of striatal projection systems by dopamine. Annu Rev Neurosci 34:441–466.

Gill KM, Grace AA (2011) Heterogeneous processing of amygdala and hippocampal inputs in the rostral and caudal subregions of the nucleus accumbens. Int J Neuropsychopharmacol 14:1301–1314.

Gong S, Zheng C, Doughty ML, Losos K, Didkovsky N, Schambra UB, Nowak NJ, Joyner A, Leblanc G, Hatten ME, Heintz N (2003) A gene expression atlas of the central nervous system based on bacterial artificial chromosomes. Nature 425:917–925.

Gore F, Schwartz EC, Brangers BC, Aladi S, Stujenske JM, Likhtik E, Russo MJ, Gordon JA, Salzman CD, Axel R (2015) Neural representations of unconditioned stimuli in basolateral amygdala mediate innate and learned responses. Cell 162:134–145.

Gracy KN, Pickel VM (1996) Ultrastructural immunocytochemical localization of the N-methyl-D-aspartate receptor and tyrosine hydroxylase in the shell of the rat nucleus accumbens. Brain Res 739:169–181.

Graziane NM, Sun S, Wright WJ, Jang D, Liu Z, Huang YH, Nestler EJ, Wang YT, Schlüter OM, Dong Y (2016) Opposing mechanisms mediate morphine- and cocaine-induced generation of silent synapses. Nat Neurosci 19:915–925.

Grewe BF, Gründemann J, Kitch LJ, Lecoq JA, Parker JG, Marshall JD, Larkin MC, Jercog PE, Grenier F, Li JZ, Lüthi A, Schnitzer MJ (2017) Neural ensemble dynamics underlying a long-term associative memory. Nature 543:670–675.

Gründemann J, Bitterman Y, Lu T, Krabbe S, Grewe BF, Schnitzer MJ, Lüthi A (2019) Amygdala ensembles encode behavioral states. Science 364: eaav8736.

Guo Q, Wang D, He X, Feng Q, Lin R, Xu F, Fu L, Luo M (2015) Whole-brain mapping of inputs to projection neurons and cholinergic interneurons in the dorsal striatum. PLoS One 10:e0123381.

Harvey J, Lacey MG (1996) Endogenous and exogenous dopamine depress EPSCs in rat nucleus accumbens in vitro via D1 receptors activation. J Physiol 492:143–154.

Harvey J, Lacey MG (1997) A postsynaptic interaction between dopamine D1 and NMDA receptors promotes presynaptic inhibition in the rat nucleus accumbens via adenosine release. J Neurosci 17:5271–5280.

Hirose K, Nakaya Y, Kitano K, Saito Y, Kaneko R, Yanagawa Y, Yamamoto K, Shirakawa T, Kobayashi M (2021) Differential regulation of medium spiny and cholinergic neurons in the nucleus accumbens core by the insular and medial prefrontal cortices in the rat. Pflugers Arch 473:1911–1924.

Janak PH, Tye KM (2015) From circuits to behaviour in the amygdala. Nature 517:284–292.

Jarzebowski P, Hay YA, Grewe BF, Paulsen O (2022) Different encoding of reward location in dorsal and intermediate hippocampus. Curr Biol 32:834–841.e5.

Ji X, Saha S, Martin GE (2015) The origin of glutamatergic synaptic inputs controls synaptic plasticity and its modulation by alcohol in mice nucleus accumbens. Front Synaptic Neurosci 7:12.

Ji X, Saha S, Kolpakova J, Guildford M, Tapper AR, Martin GE (2017) Dopamine receptors differentially control binge alcohol drinking-mediated synaptic plasticity of the core nucleus accumbens direct and indirect pathways. J Neurosci 37:5463–5474.

Johnson LR, Aylward RL, Hussain Z, Totterdell S (1994) Input from the amygdala to the rat nucleus accumbens: its relationship with tyrosine hydroxylase immunoreactivity and identified neurons. Neuroscience 61:851–865.

Josselyn SA, Köhler S, Frankland PW (2015) Finding the engram. Nat Rev Neurosci 16:521–534.

Kasai H, Ziv NE, Okazaki H, Yagishita S, Toyoizumi T (2021) Spine dynamics in the brain, mental disorders and artificial neural networks. Nat Rev Neurosci 22:407–422.

Kerr JN, Wickens JR (2001) Dopamine D-1/D-5 receptor activation is required for long-term potentiation in the rat neostriatum in vitro. J Neurophysiol 85:117–124.

Klapoetke NC, et al. (2014) Independent optical excitation of distinct neural populations. Nat Methods 11:338–346.

Klee JL, Souza BC, Battaglia FP (2021) Learning differentially shapes prefrontal and hippocampal activity during classical conditioning. Elife 10: e65456.

Kung VW, Hassam R, Morton AJ, Jones S (2007) Dopamine-dependent long term potentiation in the dorsal striatum is reduced in the R6/2 mouse model of Huntington's disease. Neuroscience 146:1571–1580.

Lansink CS, Jackson JC, Lankelma JV, Ito R, Robbins TW, Everitt BJ, Pennartz CM (2012) Reward cues in space: commonalities and differences in neural coding by hippocampal and ventral striatal ensembles. J Neurosci 32:12444–12459.

Lansink CS, Meijer GT, Lankelma JV, Vinck MA, Jackson JC, Pennartz CM (2016) Reward expectancy strengthens CA1 theta and beta band synchronization and hippocampal-ventral striatal coupling. J Neurosci 36:10598–10610.

Leathers ML, Olson CR (2017) In monkeys making value-based decisions, amygdala neurons are sensitive to cue value as distinct from cue salience. J Neurophysiol 117:1499–1511.

Lee BR, Ma Y-Y, Huang YH, Wang X, Otaka M, Ishikawa M, Neumann PA, Graziane NM, Brown TE, Suska A, Guo C, Lobo MK, Sesack SR, Wolf ME, Nestler EJ, Shaham Y, Schlüter OM, Dong Y (2013) Maturation of silent synapses in amygdala-accumbens projection contributes to incubation of cocaine craving. Nat Neurosci 16:1644–1651.

LeGates TA, Kvarta MD, Tooley JR, Francis TC, Lobo MK, Creed MC, Thompson SM (2018) Reward behaviour is regulated by the strength of hippocampus-nucleus accumbens synapses. Nature 564:258–262.

Levey AI, Hersch SM, Rye DB, Sunahara RK, Niznik HB, Kitt CA, Price DL, Maggio R, Brann MR, Ciliax BJ (1993) Localization of D1 and D2 dopamine receptors in brain with subtype-specific antibodies. Proc Natl Acad Sci U S A 90:8861–8865.

Liu C, Cai X, Ritzau-Jost A, Kramer PF, Li Y, Khaliq ZM, Hallermann S, Kaeser PS (2022) An action potential initiation mechanism in distal axons for the control of dopamine release. Science 375:1378–1385.

Liu QS, Pu L, Poo MM (2005) Repeated cocaine exposure in vivo facilitates LTP induction in midbrain dopamine neurons. Nature 437:1027–1031.

Liu Z, Wang Y, Cai L, Li Y, Chen B, Dong Y, Huang YH (2016) Prefrontal cortex to accumbens projections in sleep regulation of reward. J Neurosci 36:7897–7910.

Lobo MK, et al. (2013) ΔFosB induction in striatal medium spiny neuron subtypes in response to chronic pharmacological, emotional, and optogenetic stimuli. J Neurosci 33:18381–18395.

Ma YY, Lee BR, Wang X, Guo C, Liu L, Cui R, Lan Y, Balcita-Pedicino JJ, Wolf ME, Sesack SR, Shaham Y, Schlüter OM, Huang YH, Dong Y (2014) Bidirectional modulation of incubation of cocaine craving by silent synapse-based remodeling of prefrontal cortex to accumbens projections. Neuron 83:1453–1467.

Maguire G, Werblin F (1994) Dopamine enhances a glutamate-gated ionic current in OFF bipolar cells of the tiger salamander retina. J Neurosci 14:6094–6101.

Miyazaki I, Asanuma M, Diaz-Corrales FJ, Miyoshi K, Ogawa N (2004) Direct evidence for expression of dopamine receptors in astrocytes from basal ganglia. Brain Res 1029:120–123.

Moser EI, Moser MB, McNaughton BL (2017) Spatial representation in the hippocampal formation: a history. Nat Neurosci 20:1448–1464.

Mulder AB, Arts MP, Lopes da Silva FH (1997) Short- and long-term plasticity of the hippocampus to nucleus accumbens and prefrontal cortex pathways in the rat, in vivo. Eur J Neurosci 9:1603–1611.

Mulder AB, Hodenpijl MG, Lopes da Silva FH (1998) Electrophysiology of the hippocampal and amygdaloid projections to the nucleus accumbens of the rat: convergence, segregation, and interaction of inputs. J Neurosci 18:5095–5102.

Nagatomo K, Suga S, Saitoh M, Kogawa M, Kobayashi K, Yamamoto Y, Yamada K (2017) Dopamine D1 receptor immunoreactivity on fine processes of GFAP-positive astrocytes in the substantia nigra pars reticulata of adult mouse. Front Neuroanat 11:3.

Naha N, Li SP, Yang BC, Park TJ, Kim MO (2009) Time-dependent exposure of nicotine and smoke modulate ultrasubcellular organelle localization of dopamine D1 and D2 receptors in the rat caudate-putamen. Synapse 63:847–854.

Nicola SM, Malenka RC (1997) Dopamine depresses excitatory and inhibitory synaptic transmission by distinct mechanisms in the nucleus accumbens. J Neurosci 17:5697–5710.

Nicola SM, Kombian SB, Malenka RC (1996) Psychostimulants depress excitatory synaptic transmission in the nucleus accumbens via presynaptic D1-like dopamine receptors. J Neurosci 16:1591–1604.

Nimitvilai S, Lopez MF, Mulholland PJ, Woodward JJ (2017) Ethanol dependence abolishes monoamine and GIRK (Kir3) channel inhibition of orbitofrontal cortex excitability. Neuropsychopharmacology 42:1800–1812.

Nisenbaum ES, Mermelstein PG, Wilson CJ, Surmeier DJ (1998) Selective blockade of a slowly inactivating potassium current in striatal neurons by (+/-) 6-chloro-APB hydrobromide (SKF82958). Synapse 29:213–224.

O'Donnell P, Grace AA (1995) Synaptic interactions among excitatory afferents to nucleus accumbens neurons: hippocampal gating of prefrontal cortical input. J Neurosci 15:3622–3639.

O'Neill PK, Gore F, Salzman CD (2018) Basolateral amygdala circuitry in positive and negative valence. Curr Opin Neurobiol 49:175–183.

Pawlak V, Kerr JN (2008) Dopamine receptor activation is required for corticostriatal spike-timing-dependent plasticity. J Neurosci 28:2435–2446.

Pennartz CM, Groenewegen HJ, Lopes da Silva FH (1994) The nucleus accumbens as a complex of functionally distinct neuronal ensembles: an integration of behavioural, electrophysiological and anatomical data. Prog Neurobiol 42:719–761.

Picconi B, Centonze D, Håkansson K, Bernardi G, Greengard P, Fisone G, Cenci MA, Calabresi P (2003) Loss of bidirectional striatal synaptic plasticity in L-DOPA-induced dyskinesia. Nat Neurosci 6:501–506.

Pickel VM, Towle AC, Joh TH, Chan J (1988) Gamma-aminobutyric acid in the medial rat nucleus accumbens: ultrastructural localization in neurons receiving monosynaptic input from catecholaminergic afferents. J Comp Neurol 272:1–14.

Redondo RL, Kim J, Arons AL, Ramirez S, Liu X, Tonegawa S (2014) Bidirectional switch of the valence associated with a hippocampal contextual memory engram. Nature 513:426–430.

Reed SJ, Lafferty CK, Mendoza JA, Yang AK, Davidson TJ, Grosenick L, Deisseroth K, Britt JP (2018) Coordinated reductions in excitatory input to the nucleus accumbens underlie food consumption. Neuron 99:1260–1273.e4.

Robinson DL, Carelli RM (2008) Distinct subsets of nucleus accumbens neurons encode operant responding for ethanol versus water. Eur J Neurosci 28:1887–1894.

Schoffelmeer AN, Vanderschuren LJ, De Vries TJ, Hogenboom F, Wardeh G, Mulder AH (2000) Synergistically interacting dopamine D1 and NMDA receptors mediate nonvesicular transporter-dependent GABA release from rat striatal medium spiny neurons. J Neurosci 20:3496–3503.

Schotanus SM, Chergui K (2008) Dopamine D1 receptors and group I metabotropic glutamate receptors contribute to the induction of long-term potentiation in the nucleus accumbens. Neuropharmacology 54:837–844.

Sesack SR, Pickel VM (1990) In the rat medial nucleus accumbens, hippocampal and catecholaminergic terminals converge on spiny neurons and are in apposition to each other. Brain Res 527:266–279.

Sesack SR, Grace AA (2010) Cortico-basal ganglia reward network: microcircuitry. Neuropsychopharmacology 35:27–47.

Sesack SR, Carr DB, Omelchenko N, Pinto A (2003) Anatomical substrates for glutamate-dopamine interactions: evidence for specificity of connections and extrasynaptic actions. Ann N Y Acad Sci 1003:36–52.

Shen W, Flajolet M, Greengard P, Surmeier DJ (2008) Dichotomous dopaminergic control of striatal synaptic plasticity. Science 321:848–851.

Shuen JA, Chen M, Gloss B, Calakos N (2008) Drd1a-tdTomato BAC transgenic mice for simultaneous visualization of medium spiny neurons in the direct and indirect pathways of the basal ganglia. J Neurosci 28:2681–2685.

Smith DM, Yang YY, Subramanian DL, Miller AMP, Bulkin DA, Law LM (2022) The limbic memory circuit and the neural basis of contextual memory. Neurobiol Learn Mem 187:107557.

Tonegawa S, Morrissey MD, Kitamura T (2018) The role of engram cells in the systems consolidation of memory. Nat Rev Neurosci 19:485–498.

Totterdell S, Smith AD (1989) Convergence of hippocampal and dopaminergic input onto identified neurons in the nucleus accumbens of the rat. J Chem Neuroanat 2:285–298.

Tritsch NX, Sabatini BL (2012) Dopaminergic modulation of synaptic transmission in cortex and striatum. Neuron 76:33–50.

Trouche S, Koren V, Doig NM, Ellender TJ, El-Gaby M, Lopes-Dos-Santos V, Reeve HM, Perestenko PV, Garas FN, Magill PJ, Sharott A, Dupret D (2019) A hippocampus-accumbens tripartite neuronal motif guides appetitive memory in space. Cell 176:1393–1406.e16.

Tye KM, Stuber GD, de Ridder B, Bonci A, Janak PH (2008) Rapid strengthening of thalamo-amygdala synapses mediates cue-reward learning. Nature 453:1253–1257.

Uno M, Ozawa N (1991) Long-term potentiation of the amygdalo-striatal synaptic transmission in the course of development of amygdaloid kindling in cats. Neurosci Res 12:251–262.

van de Ven V, Lee C, Lifanov J, Kochs S, Jansma H, De Weerd P (2020) Hippocampal-striatal functional connectivity supports processing of temporal expectations from associative memory. Hippocampus 30:926–937.

Vermeulen RJ, Jongenelen CA, Langeveld CH, Wolters EC, Stoof JC, Drukarch B (1994) Dopamine D1 receptor agonists display a different intrinsic activity in rat, monkey and human astrocytes. Eur J Pharmacol 269:121–125.

Volkow ND, Wise RA, Baler R (2017) The dopamine motive system: implications for drug and food addiction. Nat Rev Neurosci 18:741–752.

Wang J, Ishikawa M, Yang Y, Otaka M, Kim JY, Gardner GR, Stefanik MT, Milovanovic M, Huang YH, Hell JW, Wolf ME, Schlüter OM, Dong Y (2018) Cascades of homeostatic dysregulation promote incubation of cocaine craving. J Neurosci 38:4316–4328.

Warren BL, Suto N, Hope BT (2017) Mechanistic resolution required to mediate operant learned behaviors: insights from neuronal ensemble-specific inactivation. Front Neural Circuits 11:28.

Weymar M, Schwabe L (2016) Amygdala and emotion: the bright side of it. Front Neurosci 10:224.

Wise RA (2004) Dopamine, learning and motivation. Nat Rev Neurosci 5:483–494.

Wolosin SM, Zeithamova D, Preston AR (2012) Reward modulation of hippocampal subfield activation during successful associative encoding and retrieval. J Cogn Neurosci 24:1532–1547.

Wright WJ, Dong Y (2021) Silent synapses in cocaine-associated memory and beyond. J Neurosci 41:9275–9285.

Wright WJ, Graziane NM, Neumann PA, Hamilton PJ, Cates HM, Fuerst L, Spenceley A, MacKinnon-Booth N, Iyer K, Huang YH, Shaham Y, Schlüter OM, Nestler EJ, Dong Y (2020) Silent synapses dictate cocaine memory destabilization and reconsolidation. Nat Neurosci 23:32–46.

Xia SH, Yu J, Huang X, Sesack SR, Huang YH, Schlüter OM, Cao JL, Dong Y (2020) Cortical and thalamic interaction with amygdala-to-accumbens synapses. J Neurosci 40:7119–7132.

Xu TX, Yao WD (2010) D1 and D2 dopamine receptors in separate circuits cooperate to drive associative long-term potentiation in the prefrontal cortex. Proc Natl Acad Sci U S A 107:16366–16371.

Yagishita S, Hayashi-Takagi A, Ellis-Davies GC, Urakubo H, Ishii S, Kasai H (2014) A critical time window for dopamine actions on the structural plasticity of dendritic spines. Science 345:1616–1620.

Yu J, Yan Y, Li KL, Wang Y, Huang YH, Urban NN, Nestler EJ, Schlüter OM, Dong Y (2017) Nucleus accumbens feedforward inhibition circuit promotes cocaine self-administration. Proc Natl Acad Sci U S A 114:E8750–E8759.

Yu J, Ishikawa M, Wang J, Schlüter OM, Sesack SR, Dong Y (2019) Ventral tegmental area projection regulates glutamatergic transmission in nucleus accumbens. Sci Rep 9:18451.

Zanassi P, Paolillo M, Montecucco A, Avvedimento EV, Schinelli S (1999) Pharmacological and molecular evidence for dopamine D(1) receptor expression by striatal astrocytes in culture. J Neurosci Res 58:544–552.

Zhang JC, Lau PM, Bi GQ (2009) Gain in sensitivity and loss in temporal contrast of STDP by dopaminergic modulation at hippocampal synapses. Proc Natl Acad Sci U S A 106:13028–13033.

Zhang L, Bose P, Warren RA (2014) Dopamine preferentially inhibits NMDA receptor-mediated EPSCs by acting on presynaptic D1 receptors in nucleus accumbens during postnatal development. PLoS One 9:e86970.

Zhang X, Guan W, Yang T, Furlan A, Xiao X, Yu K, An X, Galbavy W, Ramakrishnan C, Deisseroth K, Ritola K, Hantman A, He M, Josh Huang Z, Li B (2021) Genetically identified amygdala-striatal circuits for valence-specific behaviors. Nat Neurosci 24:1586–1600.

Zhou FM, Wilson C, Dani JA (2003) Muscarinic and nicotinic cholinergic mechanisms in the mesostriatal dopamine systems. Neuroscientist 9:23–36.

Zinsmaier AK, Dong Y, Huang YH (2022) Cocaine-induced projection-specific and cell type-specific adaptations in the nucleus accumbens. Mol Psychiatry 27:669–686.